Supporting Information for

Assessment of the combined radiative effects of black carbon in the atmosphere and snowpack in the Northern Hemisphere constrained by surface observations

Tenglong Shi[a], Yang Chen[a], Yuxuan Xing[a], Xiaoying Niu[a], Dongyou Wu[a], Jiecan Cui[a], Yue Zhou[a], Wei Pu[a], and Xin Wang*[ab]

*Corresponding author

[a]Key Laboratory for Semi-Arid Climate Change of the Ministry of Education, College of Atmospheric Sciences, Lanzhou University, Lanzhou 730000, China. E-mail: wxin@lzu.edu.cn

[b]School of Earth System Science, Tianjin University, Tianjin 300072, China

Contents of this file

S1 - Inputs for atmospheric and snow radiative transfer model

Input parameters for the Fu–Liou radiative transfer model (RTM) typically include the meteorological variables temperature, pressure, humidity, and ozone concentration as well as aerosol profiles and aerosol optical depth at the wavelength of 0.55 μm. Additional required input includes cloud property profiles (i.e., liquid water content, ice water content, effective radius of water cloud, and effective diameter of ice cloud) and surface albedo.

We obtained monthly pressure-level meteorological variables (temperature, pressure, humidity, ozone concentration) from the Modern-Era Retrospective Analysis for Research and Applications, Version 2 (MERRA-2) datasets (product: instM_3d_asm_Np). The horizontal resolution of the dataset is 0.5° × 0.625°; vertical resolution comprises 42 levels spread between the surface and an altitude of 80 km. MERRA-2 is a new reanalysis data released in 2017 by NASA's Global Modeling and Assimilation Office (GMAO).[1] It's based on the Goddard Earth Observing System Model, Version 5 (GEOS-5) and Data Assimilation System, Version 5.12.4 (ADAS-5.12.4).[2] The MERRA-2 data is available online through the Goddard Earth Sciences (GES) Data and Information Services Center (DISC) (https://disc.gsfc.nasa.gov).

The BC profile and optical depth at 0.55 μm used in this study were also derived from the MEAAR-2 datasets (product: inst3_3d_aer_Nv and tavgM_2d_aer_Nx). Here we average the 3-hourly BC mixing ratio data on a monthly scale, and interpolate the initial 72 pressure layers in the vertical direction to 42 pressure layers, corresponding to the vertical layers of the meteorological variables. In addition, several AOD datasets are assimilated and absorbed by MERRA-2, including bias-corrected AOD of the Moderate Resolution Imaging Spectrometer (MODIS), the Advanced Very High Resolution Radiometer (AVHRR) instruments, AOD retrievals from the Multiangle Imaging SpectroRadiometer (MISR) over bright surfaces, and ground-based Aerosol Robotic Network (AERONET) direct measurements of AOD.[1, 3] Therefore, the MERRA-2 AOD datasets are relatively reliable.[4]

The cloud microphysical parameters, including liquid water content (LWC), ice water content (IWC), effective radius of water cloud particles, and effective diameter of ice cloud particles, were obtained from the monthly CERES SYN1deg Ed4A product (hereinafter CERES, the Clouds and the Earth's Radiant Energy System).[5] Which are derived by combining cloud properties measured by the MODIS sensor on board the Terra and Aqua platforms and geostationary satellite (GEO) images.[6] The product also provides four cloud types: low-level clouds (surface–700 hPa), lower mid-level clouds (700–500 hPa), higher mid-level clouds (500–300 hPa), and high-level clouds (300–50 hPa). The exact location of cloud layers is determined by its effective pressure.

The clear- (α_{clear}) and cloudy-sky (α_{cloudy}) surface albedo (i.e., snow albedo) at 6 bands (0.2–0.7, 0.7–1.3, 1.3–1.9, 1.9–2.5, 2.5–3.5, and 3.5–4.0 μm) was simulated by the Snow, Ice, and Aerosol Radiative (SNICAR) model under clear and cloudy sky conditions, respectively, with a R_{ef} of 200 (1000) μm for fresh (old) snow in the autumn–winter (spring–summer) season. Meanwhile, we assumed a soil albedo of 0.3 for the bottom layer, representing the reflection properties beneath the snowpack. The other input parameters for SNICAR include snow thickness and density and the BC content of the snow (BC_S). Here, snow thickness and density values are derived from MERRA-2 data (product: tavgM_2d_lnd_Nx), and BC_S values are obtained from the Coupled Model Intercomparison Project Phase 6 (CMIP6) historical experiment results. Here we collect a total of 7 model results (i.e., CESM2_historical, CESM2-FV2_historical, CESM2-WACCM_historical, CESM2-WACCM-FV2_historical, NorESM2-LM_historical, NorESM2-MM_historical, and TaiESM1_historical), and then give the results of the multi-model averages. Eyring et al.[7] has presented a comprehensive description on the CMIP6 experimental design and organization, the CMIP6 results are publicly available at https://esgf-node.llnl.gov/search/cmip6/. For this study, we employed the multi-model average monthly BC_S output for the period 2010–2014 to drive the SNICAR model. Finally, the all-sky snow albedo ($\alpha_{all-sky}$) as inputs for Fu-Liou model was then calculated based on weighted clear- and cloudy-sky albedo values depending on the cloud fraction (CF) (i.e., $\alpha_{all-sky} = CF \times \alpha_{cloudy} + (1 - CF) \times \alpha_{clear}$), and the data of CF were obtained from the Clouds and the Earth's Radiant Energy System (CERES) (https://ceres.larc.nasa.gov/products.php?product=SYN1deg). In addition, all other products used in this study are also for the year 2010-2014 and, unless otherwise stated, have been remapped to 2.5° × 1.875° resolution to match CMIP6 model results.

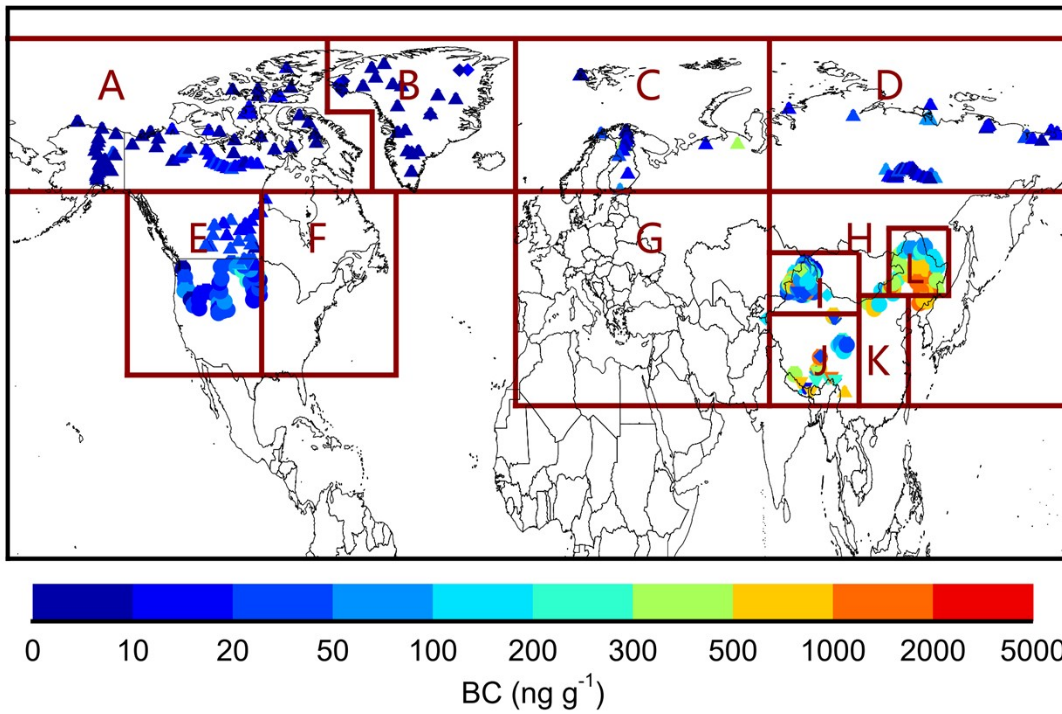

Figure S1. Spatial distribution of the measured black carbon (BC) concentration across the Northern Hemisphere. Here the Northern Hemisphere are separated into twelve study regions, and regions are labelled in order from A to L.

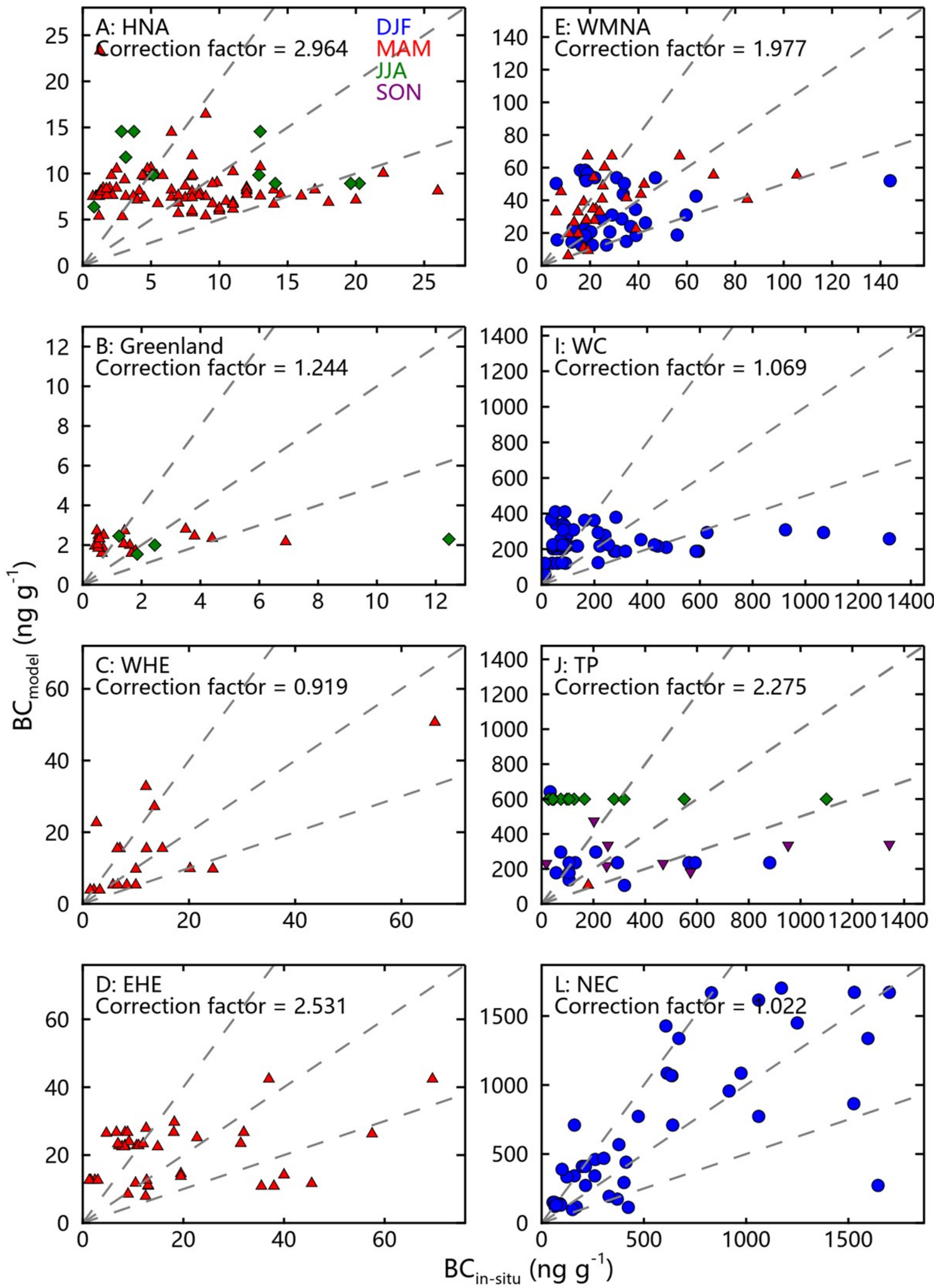

Figure S2. Comparison of the snowpack BC measurements and CMIP6 multi-model averaged BC concentrations in the HNA, Greenland, WHE, EHE, WMNA, WC, TP, and NEC.

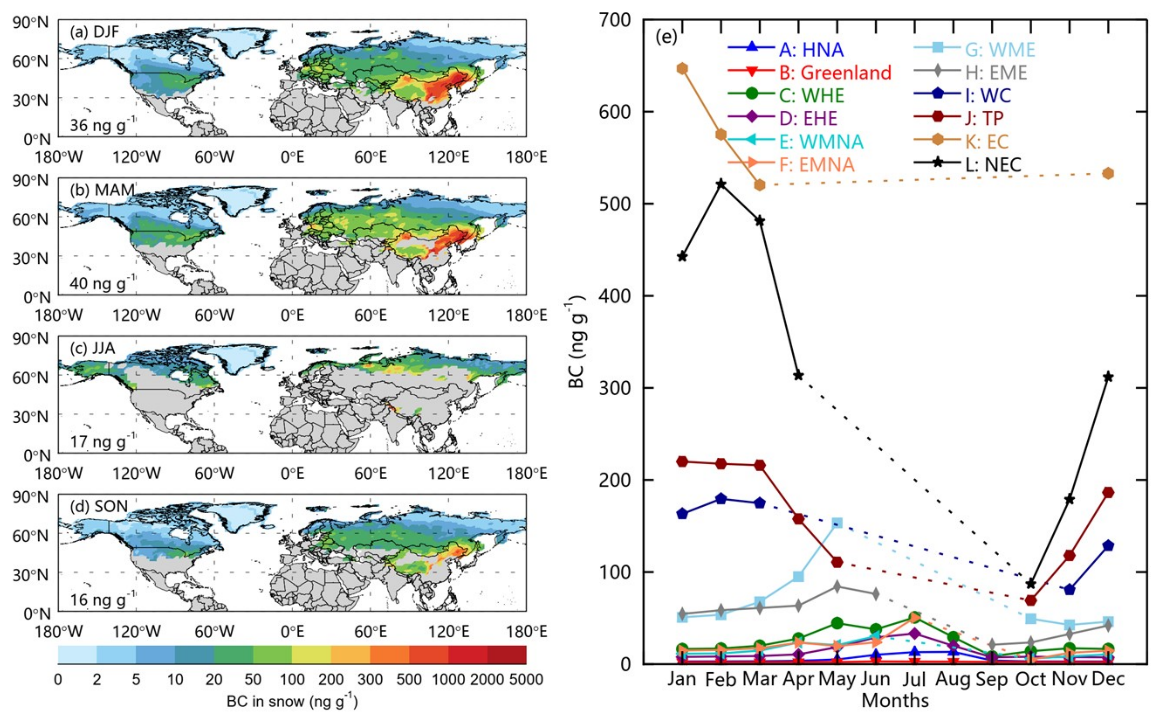

Figure S3. Spatial distributions of mean seasonal snow BC contents in the Northern Hemisphere for (a) DJF, (b) MAM, (c) JJA, and (d) SON during 2010–2014. Regional averages for the entire hemisphere are shown in the bottom left corner of each panel. (e) Mean monthly BC_S for each region.

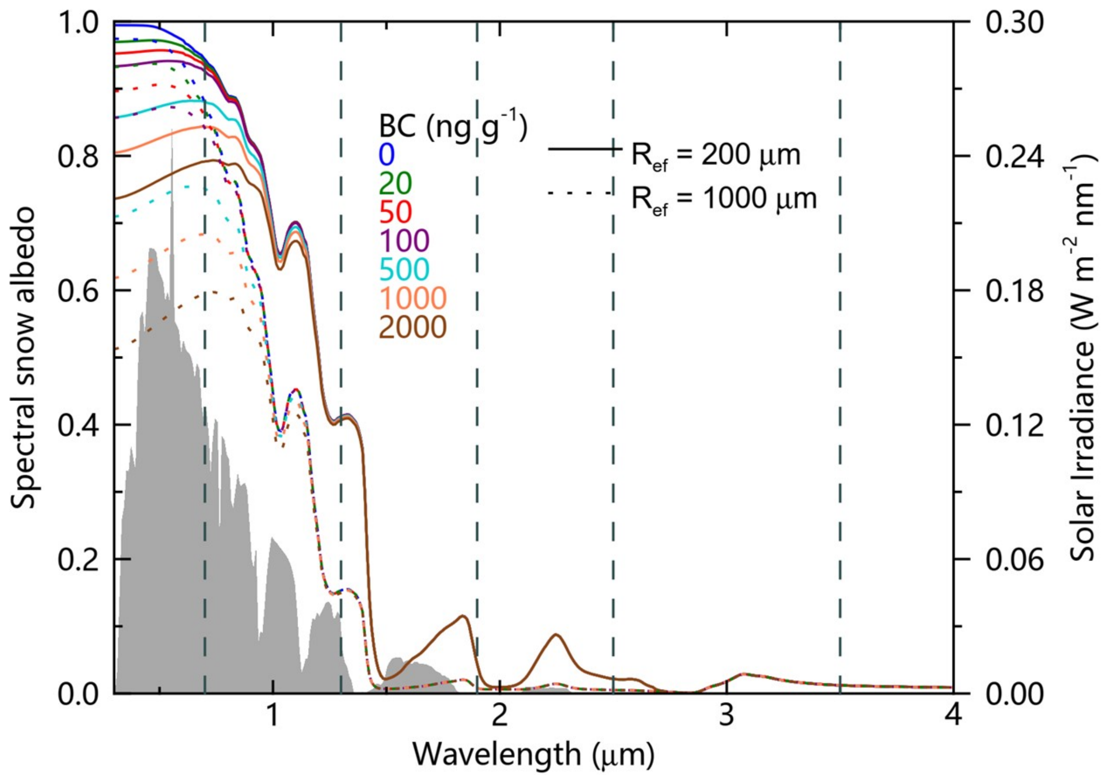

Figure S4. Spectral snow albedo simulated by the SNICAR model with 0, 20, 50, 100, 500, 1000, and 2000 ng g^{-1} of BC contamination for fresh snow (solid line) and old snow (dotted line), under cloudy sky conditions. Gray areas denote the typical spectral solar irradiance for mid-latitude winter. Fu–Liou bands at the solar spectra (0.2–0.7, 0.7–1.3, 1.3–1.9, 1.9–2.5, 2.5–3.5, and 3.5–4.0 μm) are shown separated by gray dashed lines.

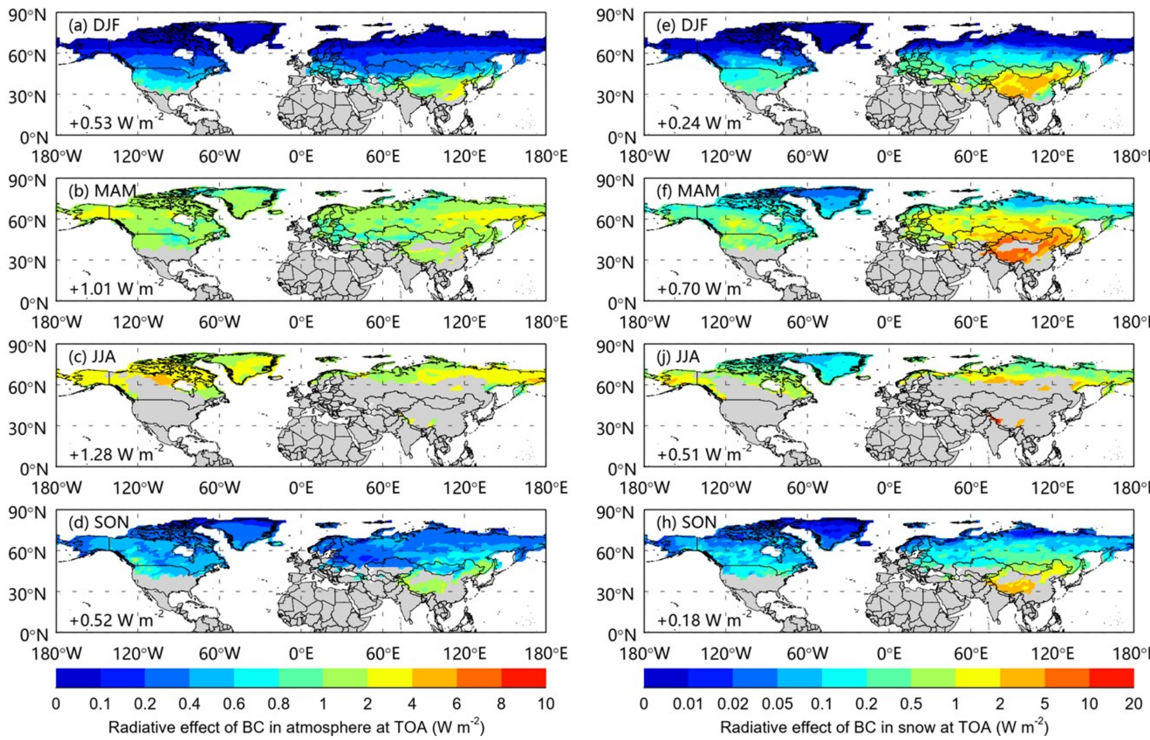

Figure S5. Spatial distributions of mean seasonal radiative effect of (a–d) atmospheric BC (RE_{atmo}^{TOA}) and (e–f) snow BC (RE_{snow}^{TOA}) over the Northern Hemisphere in 2017 at the TOA. Regional averages for the Northern Hemisphere are shown in the bottom left corner of each panel.

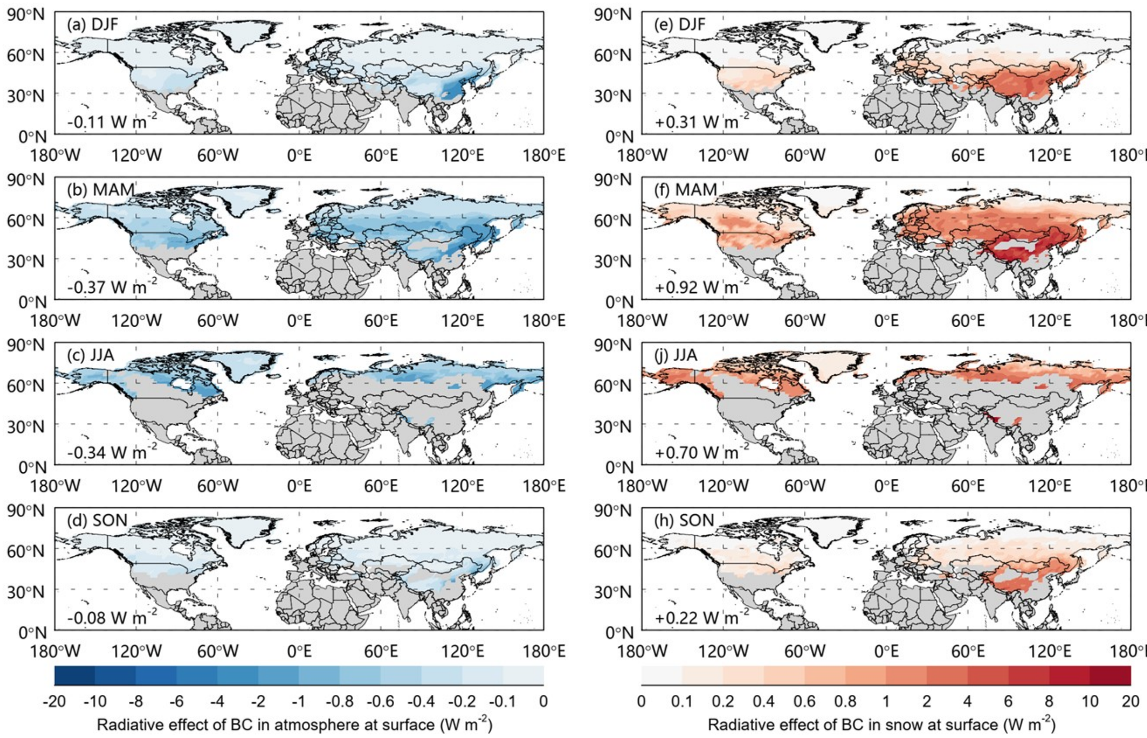

Figure S6. As for Figure S3, but depicting (a–d) atmospheric BC (RE_{atmo}^{Sur}) and (e–f) snow BC (RE_{snow}^{Sur}) radiative effect at the surface.

Table S1. The correction factor of CMIP6 averaged BC concentrations in snow for different regions.

Region	Correction factor
A: HNA	2.964
B: Greenland	1.244
C: WHE	0.919
D: EHE	2.531
E: WMNA	1.977
F: EMNA	1.977
G: WME	0.994
H: EME	1.069
I: WC	1.069
J: TP	2.275
K: EC	1.022
L: NEC	1.022

References

1. C. A. Randles, A. M. Da Silva, V. Buchard, P. R. Colarco, A. Darmenov, R. Govindaraju, A. Smirnov, B. Holben, R. Ferrare, J. Hair, Y. Shinozuka and C. J. Flynn, The MERRA-2 Aerosol Reanalysis, 1980 Onward. Part I: System Description and Data Assimilation Evaluation, *J Climate*, 2017, **30**, 6823-6850.
2. V. Buchard, C. A. Randles, A. M. da Silva, A. Darmenov, P. R. Colarco, R. Govindaraju, R. Ferrare, J. Hair, A. J. Beyersdorf, L. D. Ziemba and H. Yu, The MERRA-2 Aerosol Reanalysis, 1980 Onward. Part II: Evaluation and Case Studies, *J Climate*, 2017, **30**, 6851-6872.
3. B. N. Holben, T. F. Eck, I. Slutsker, D. Tanre, J. P. Buis, A. Setzer, E. Vermote, J. A. Reagan, Y. J. Kaufman, T. Nakajima, F. Lavenu, I. Jankowiak and A. Smirnov, AERONET - A federated instrument network and data archive for aerosol characterization, *Remote Sens Environ*, 1998, **66**, 1-16.
4. C. A. Gueymard and D. Z. Yang, Worldwide validation of CAMS and MERRA-2 reanalysis aerosol optical depth products using 15 years of AERONET observations, *Atmospheric Environment*, 2020, **225**.
5. P. Minnis, G. Hong, S. Sun-Mack, W. L. Smith, Y. Chen and S. D. Miller, Estimating nocturnal opaque ice cloud optical depth from MODIS multispectral infrared radiances using a neural network method, *J Geophys Res-Atmos*, 2016, **121**, 4907-4932.
6. P. Minnis, S. Sun-Mack, D. F. Young, P. W. Heck, D. P. Garber, Y. Chen, D. A. Spangenberg, R. F. Arduini, Q. Z. Trepte, W. L. Smith, J. K. Ayers, S. C. Gibson, W. F. Miller, G. Hong, V. Chakrapani, Y. Takano, K. N. Liou, Y. Xie and P. Yang, CERES Edition-2 Cloud Property Retrievals Using TRMM VIRS and Terra and Aqua MODIS Data—Part I: Algorithms, *Ieee T Geosci Remote*, 2011, **49**, 4374-4400.
7. V. Eyring, S. Bony, G. A. Meehl, C. A. Senior, B. Stevens, R. J. Stouffer and K. E. Taylor, Overview of the Coupled Model Intercomparison Project Phase 6 (CMIP6) experimental design and organization, *Geosci Model Dev*, 2016, **9**, 1937-1958.